

See discussions, stats, and author profiles for this publication at: <https://www.researchgate.net/publication/221827907>

Structural Identification of a Novel Axially Chiral Binaphthyl Fluorene Based Salen Ligand in Solution Using Electronic Circular Dichroism: A Theoretical Experimental Analysis

ARTICLE *in* THE JOURNAL OF PHYSICAL CHEMISTRY A · FEBRUARY 2012

Impact Factor: 2.69 · DOI: 10.1021/jp2112507 · Source: PubMed

CITATIONS

4

READS

7

6 AUTHORS, INCLUDING:



Carlos Diaz

University of Colorado Colorado Springs

15 PUBLICATIONS 53 CITATIONS

[SEE PROFILE](#)



Alma R Morales

University of Central Florida

45 PUBLICATIONS 907 CITATIONS

[SEE PROFILE](#)



Kevin D Belfield

University of Central Florida

225 PUBLICATIONS 4,268 CITATIONS

[SEE PROFILE](#)



Supriyo Ray

University of California, San Diego

12 PUBLICATIONS 77 CITATIONS

[SEE PROFILE](#)

Structural Identification of a Novel Axially Chiral Binaphthyl Fluorene Based Salen Ligand in Solution Using Electronic Circular Dichroism: A Theoretical–Experimental Analysis

Carlos Diaz,[†] Andrew Frazer,[†] Alma Morales,[†] Kevin D. Belfield,^{†,‡} Supriyo Ray,[§] and Florencio E. Hernández*,^{†,‡}

[†]Department of Chemistry, University of Central Florida, P.O. Box 162366, Orlando, Florida 32816-2366, United States

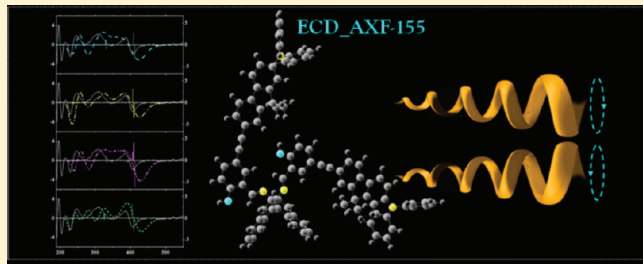
[‡]The College of Optics and Photonics, CREOL, University of Central Florida, P.O. Box 162366, Orlando, Florida 32816-2366, United States

[§]Department of Physics, University of Central Florida, P.O. Box 162385, Orlando, Florida 32816-2385, United States

S Supporting Information

ABSTRACT: A novel axially chiral binaphthyl fluorene based salen ligand, AFX-155 [2,2'-(1E,1'E)-(R)-1,1'-binaphthyl-2,2'-diylbis(azan-1-yl-1-ylidene)bis(methan-1-yl-1-ylidene)bis(4-((7-(diphenylamino)-9,9-dihexyl-9H-fluoren-2-yl)ethynyl)-phenol)], with potential applications in homogeneous catalysis, biophotonics, and sensing was synthesized. A full comparative theoretical–experimental analysis of the UV–vis and electronic circular dichroism (ECD) spectra of the 10 primary isomers, comprising stereoisomers and optical isomers, revealed the presence of the unique structure in tetrahydrofuran (THF) solution, the *trans-R-intra*//*trans-R-extra*. A proposed route of attack of the (R)-(+)-2,2'-diamino-1,1'-binaphthalene onto a salicaldehyde 5-(2-(2-(diphenylamino)-9,9-dihexyl-9H-fluoren-7-yl)ethynyl)-2-hydroxybenzaldehyde followed by a consecutive attack of the resulting species onto another salicaldehyde, both via Burgi:Dunitz trajectory, validates the unambiguous formation of the established isomer. Steric hindrances seem to be the determinant factor that defines the 3D structural conformation of this particular stereoisomer of AFX-155 with triple axial chirality.

The determination of every optimal structure and the dominant conformers of AFX-155 were calculated evaluating, in CONFLEX, their steric energies using force fields at MMFF94S (2006-11-24HGTEMP) level in gas phase. The geometry of the conformers was optimized in THF (using PCM) using Gaussian 09 at the DFT/B3LYP level of theory and 6-31G* basis set. The first 100 electronic excited states were calculated using the same level of theory and basis set.



INTRODUCTION

The discovery of privileged chiral ligands such as (R)-BINAP, (R)-BINOL, and (R,R)-salen, which exhibit high selectivity over a broad range of reactions,^{1–4} has enabled the development of practical applications for catalytic asymmetric processes in fundamental and applied research as well as in industry.^{5,6} The main advantage of using the first two ligands resides on their extraordinary selectivity imposed by the atropisomerism on the C₂ symmetry framework with axial chirality, which limits the racemization. The major benefit of using the latter in asymmetric reactions is the typical high yield synthetic accessibility of enantiopure derivatives by the condensation of salicylic aldehydes with diamines of definite chirality. The precise catalyst steric and electronic property of specifically designed chelating ligands that bridges metal ions with two nitrogen and two oxygen atoms (salen ligands) for a broad range of catalytic asymmetric reactions and with important applications in the pharmaceutical and chemical industries⁷ strongly depends on their structure.

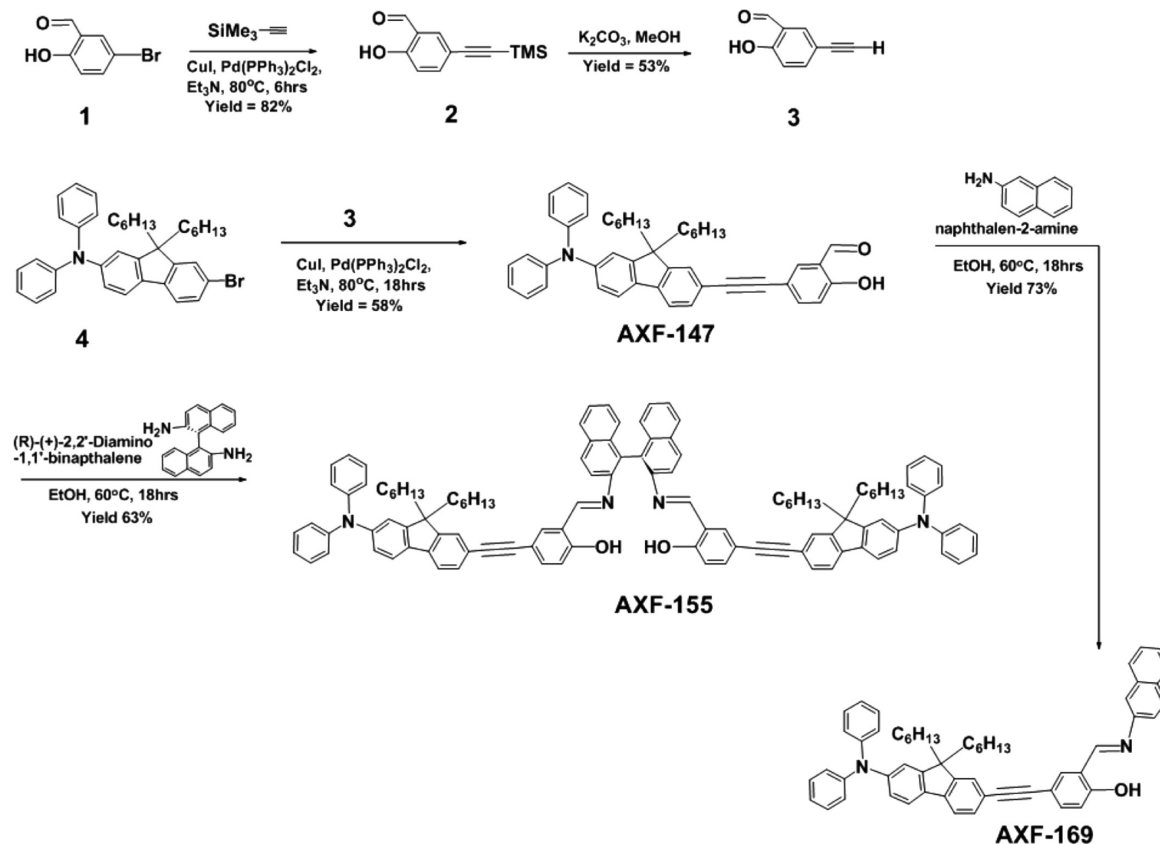
Although a large number of ligand structures have been studied during recent decades,^{8–13} there is still a relative modest understanding about salen-type ligands with multiple sources of chirality into the ligand backbone to enhance the reaction possibility and selectivity of these catalysts.^{14,15} Furthermore, the challenges involved in the synthesis of helical-type salen complexes have not permitted the study of twisted structures. In this respect, Wiznycia et al. have recently reported on the synthesis and structural characterization of the first monohelical salen complexes with predetermined handedness.^{16–18} These authors were able to produce, for the very first time, a multidentate ligand by the condensation of (R)-(+)-1,1'-binaphthyl-2,2'-diamine with 1,1-binaphthyl-2,2'-diamine in ethanol. Using X-ray crystallography, Wiznycia et al. accurately determined the helicity as well as the handedness of a crystal of the monohelical complex of Fe^{II} and Zn^{II} and demonstrated

Received: November 22, 2011

Revised: February 7, 2012

Published: February 13, 2012

Scheme 1. Steps for the Synthesis of AFX-147, AFX-155, and AFX-169



that the 1,1-binaphthyl backbone is an effective helix-forming unit. This unique work shows that the synthesis and structural study of new salen ligands with multiple chirality and helicity is in great need to truly understand their full ability in catalytic asymmetric processes important in industry. Exploring further the potential of using 1,1-binaphthyl backbone in the synthesis of these specific ligands as well as determining their 3D structural conformation in solution is in great demand.

Herein, we report on the structural characterization of a recently synthesized axially chiral binaphthyl fluorene based salen ligand, AFX-155 [2,2'-(1E,1'E)-(R)-1,1'-binaphthyl-2,2'-diylbis(azan-1-yl-1-ylidene)bis(methan-1-yl-1-ylidene)bis(4-((7-(diphenylamino)-9,9-dihexyl-9H-fluoren-2-yl)ethynyl)-phenol)], with potential applications in homogeneous catalysis, biophotonics, and sensing. The full comparative theoretical–experimental analysis of the UV–vis and electronic circular dichroism (ECD) spectra of the primary isomers, comprising stereoisomers and optical isomers, revealed the presence of the unique *trans-R-intra*//*trans-R-extra*. The analysis of the theoretical–experimental results has permitted us to determine the 3D structural conformation of AFX-155 in tetrahydrofuran (THF) solution and to propose a preferential route of attack of the (R)-(+)-2,2'-diamino-1,1'-binaphthalene onto a salicaldehyde 5-(2-(diphenylamino)-9,9-dihexyl-9H-fluoren-7-yl)ethynyl-2-hydroxybenzaldehyde followed by a consecutive attack of the resulting species onto another salicaldehyde both via Burgi:Dunitz trajectory.¹⁹ The substantiation of the important steric hindrances, throughout the condensation phase, validates the unambiguous formation of the particular stereoisomer of AFX-155 with triple axial chirality and distorted helicity.

SYNTHESIS OF AFX-155

We synthesized a new chiral chromophore (see Scheme 1) of the D– π –A– π –D type, where A represents an electron-withdrawing moiety while $-\pi-$ represents a conjugated π -electron system. D symbolizes a well-known donor group, a fluorene moiety attached to a diphenylamino group. On the opposite arm of the fluorene, in the 2 position, there is an alkyne bond connected to a phenyl ring. The fluorene hexyl groups in position 9 augment the solubility in hydrophobic environments.

A fluorene derivative was specifically chosen for this synthesis because of its extended π -electron delocalization that confers (a) high nonlinear absorption cross section,^{20–25} (b) rigid fluorene core that grants exceptional thermal- and photo-stability,^{26–28} (c) high fluorescence quantum yield (>0.5) required for bioimaging,²³ (d) very low cytotoxicity necessary for practical biomedical applications,^{28,29} and (e) a typical linear absorption maxima between 350 and 450 nm exceptional for multiphoton excitation.^{30–32}

The key step for the synthesis of this fluorenyl probe, AFX-155, was a Pd catalyzed Sonogashira coupling reaction (Scheme 1), which comprises the coupling of the previously described 5-ethynyl-2-hydroxybenzaldehyde (3) with a 7-bromo-9,9-dihexyl-N,N-diphenyl-9H-fluoren-2-amine (4) to yield the salicaldehyde 5-(2-(diphenylamino)-9,9-dihexyl-9H-fluoren-7-yl)ethynyl-2-hydroxybenzaldehyde (AFX-147). The condensation of the novel fluorene based salicaldehyde with the R enantiomer of the binaphthyl diamine (R)-(+)-2,2'-diamino-1,1'-binaphthalene resulted in the formation of this new binaphthyl based salen compound in good overall yield (63%).

All compounds were fully characterized by ^1H NMR, ^{13}C NMR, and elemental analysis or HR-MS.

Materials and Synthetic Procedures. The syntheses of 5-ethynyl-2-hydroxybenzaldehyde (**3**) and 7-bromo-9,9-dihexyl-N,N-diphenyl-9H-fluoren-2-amine (**4**) have been described previously.^{33–35} Pd catalyzed reactions were performed in high-pressure Schlenk tubes under N_2 atmosphere. All reagents and solvents were used as received from commercial suppliers unless otherwise noted. ^1H and ^{13}C NMR spectroscopic measurements were performed using a Varian 500 NMR spectrometer at 500 MHz with tetramethylsilane (TMS) as internal reference: ^1H (referenced to TMS at $\delta = 0.0$ ppm) and ^{13}C (referenced to CDCl_3 at $\delta = 77.0$ ppm). High-resolution mass spectrometry (HR-MS) analysis was performed in the Department of Chemistry, University of Florida, Gainesville, FL.

Synthesis of Salicaldehyde 5-(2-(2-(diphenylamino)-9,9-dihexyl-9H-fluoren-7-yl)ethynyl)-2-hydroxybenzaldehyde AXF-147. To 30 mL of a solution of the 7-bromo-9,9-dihexyl-N,N-diphenyl-9H-fluoren-2-amine (**D**) (1.24 g, 2.14 mmol) in THF:triethylamine (50:50), we added 15.0 mg of CuI (0.08 mmol) and $\text{Pd}(\text{PPh}_3)_2\text{Cl}_2$ (0.07 mmol). Then, 20 mL of a solution of 5-ethynyl-2-hydroxybenzaldehyde (0.48 g, 3.29 mmol) in THF was added to the mixture. The resultant slurry was then heated at 80 °C for 8 h. Afterward, the reaction mixture was allowed to cool to ambient temperature before filtering it through Celite. The Celite was then washed twice with 30 mL of THF. The combined filtrates had all volatile residues removed under reduced vacuum. The recovered final product was a red oil. The purification of this product was then performed using a silica gel column as the stationary phase and eluting with hexane and ethylacetate 1:9 (mobile phase). The isolated pure orange oil was subject to constant vacuum over a period of 24 h to yield an orange solid (yield 0.80 g, 58%), mp 59–61 °C. ^1H NMR CDCl_3 (500 MHz): δ (ppm) = 11.14(s, 1H, O—H), 9.92(d, 1H, $\text{HC}=\text{O}$), 7.81(d, 1H), 7.72(dd, 1H), 7.61–7.56(m, 2H), 7.50–7.45(2H), 7.29–7.26(m, 6H), 7.15–7.12(m, 5H), 7.05–7.01(m, 4H), 1.91–1.85(m, 4H), 1.17–1.07(m, 12H), 0.82(t, 6H), 0.67(m, 4H). ^{13}C NMR(500 MHz): δ (ppm) = 196.35 ($\text{HC}=\text{O}$), 161.52 (C—OH), 152.70, 150.98, 148.11, 147.91, 141.71, 140.00, 136.99, 135.56, 130.84, 129.44, 125.92, 124.20, 123.62, 122.92, 120.97, 120.79, 120.33, 119.29, 119.22, 118.38, 115.77, 90.44, 87.59, 55.34, 40.47, 31.77, 29.86, 23.98, 22.80, 14.27; MS (HR-ESI) calculated for $\text{C}_{46}\text{H}_{47}\text{NO}_2$ ($M + \text{H}^+$) 646.36; found ($M + \text{H}^+$) 646.36.

Synthesis of Chiral Fluorene Compound 2,2'-(1E,1'E)-(R)-1,1'-Binaphthyl-2,2'-diylbis(azan-1-yl-1-ylidene)bis(methan-1-yl-1-ylidene)bis(4-((7-(diphenylamino)-9,9-dihexyl-9H-fluoren-2-yl)ethynyl)phenol) AXF-155. To a slurry of 5-((7-(diphenylamino)-9,9-dihexyl-9H-fluoren-2-yl)ethynyl)-2-hydroxybenzaldehyde (AXF-147) (200 mg, 0.31 mmol) in ethanol (7.0 mL), we added slowly and at room temperature 5.0 mL of a solution of (R)-(+)-2,2'-diamino-1,1'-binaphthalene (44 mgs, 0.15 mmol) in ethanol. The reaction mixture temperature was then increased to 70 °C and was kept constant for 18 h using Dean–Stark conditions. A yellow solution was recuperated after the solid was dissolved. Subsequently, the reaction mixture was halted and was taken back to ambient temperature. After filtering the precipitate, we recovered a dark-orange powder. The purification of this final product was performed using a silica gel column as the stationary phase and was eluted with hexane: ethylacetate 2:1 (mobile phase). A bright orange solid was isolated (yield 0.112

g, 63%), mp 112–113 °C. ^1H NMR CDCl_3 (500 MHz): δ (ppm) = 12.37(s, 2H, O—H), 8.72(s, 2H, $\text{HC}=\text{N}$), 8.16(d, 2H), 8.01(d, 2H), 7.70(d, 2H), 7.55–7.37(m, 20H), 7.26–7.22(m, 6H), 7.12–7.20(m, 10H), 7.03–6.98(m, 6H), 6.72(d, 2H), 2.05(m, 8H), 1.26(m, 16H), 0.79(t, 8H). ^{13}C NMR CDCl_3 (500 MHz): δ (ppm) = 158.21, 158.16, 149.75, 147.95, 145.21, 144.81, 140.57, 140.39, 138.37, 133.22, 132.82, 132.61, 130.52, 129.99, 127.82, 127.52, 127.24, 126.49, 125.68, 124.50, 123.76, 123.51, 122.90, 121.21, 120.74, 117.96, 117.92, 116.56, 116.38, 116.30, 114.90, 113.84, 111.20, (86.56, 85.77) $\text{C}\equiv\text{C}$, 52.38, 37.53, 28.84, 26.93, 21.04, 19.88, 11.35. MS (HR-ESI) calculated for $\text{C}_{112}\text{H}_{106}\text{N}_4\text{O}_2$ ($M + \text{H}^+$) 1538.83; found ($M + \text{Na}^+$) 1560.79.

Synthesis of (E)-4-((7-(Diphenylamino)-9,9-dihexyl-9H-fluoren-2-yl)ethynyl)-2-((naphthalen-2-ylimino)methyl)phenol AXF-169. To a slurry of 5-((7-(diphenylamino)-9,9-dihexyl-9H-fluoren-2-yl)ethynyl)-2-hydroxybenzaldehyde (AXF-147) (100 mg, 0.16 mmol) in ethanol (4.0 mL), we slowly added at room temperature 3.0 mL of a solution of naphthalen-2-amine (22 mgs, 0.16 mmol) in ethanol. Afterward, the temperature of the reaction mixture was raised to 70 °C and was held constant for 18 h under Dean–Stark conditions. After the solid was dissolved, a yellow solution was formed. Then, the mixture was halted and was brought to ambient temperature. A dark-orange powder was recovered and was washed with hexane. The final product was dried in vacuum and was characterized with no further purification. An orange solid was finally isolated (yield 87 mgs, 73%). mp 71–73 °C. ^1H NMR CDCl_3 (500 MHz): δ (ppm) = 13.64(s, 1H, O—H), 8.77(s, 1H, $\text{HC}=\text{N}$), 7.93–7.86(m, 3H), 7.73–7.69(m, 2H), 7.61–7.45(m, 9H), 7.23–7.04(m, 12H), 1.88(m, 4H), 1.08(m, 12H), 0.80(t, 6H), 0.66(m, 4H). ^{13}C NMR CDCl_3 (500 MHz): δ (ppm) = 158.21($\text{N}=\text{C}$), 149.75(C—OH), 147.95, 145.21, 144.81, 140.57, 140.39, 138.37, 133.22, 132.82, 132.61, 130.52, 129.99, 127.82, 127.52, 127.24, 126.49, 125.68, 124.50, 123.76, 123.51, 122.90, 121.21, 120.74, 117.96, 117.92, 116.56, 116.38, 116.30, 113.84, 111.20, (86.56, 85.77) $\text{C}\equiv\text{C}$, 52.38 (C9), 37.53, 28.84, 26.93, 21.04, 19.88, 11.35. MS (HR-ESI) calculated for $\text{C}_{56}\text{H}_{54}\text{N}_2\text{O}$ ($M + \text{H}^+$) 771.42; found ($M + \text{H}^+$) 771.42.

■ EXPERIMENTAL METHODS

All measurements were performed in THF solution. The linear absorption spectra were taken using a single-beam spectrophotometer (Agilent 8453 Diode Array UV-vis) from 190 to 600 nm in a 0.1 cm quartz cell and at a concentration of 1.5×10^{-4} M. ECD spectra were recorded on a J-810 CD spectropolarimeter (Jasco Corp., Tokyo, Japan) under the following conditions: concentration 1×10^{-3} M; temperature 25 °C; quartz cuvette length 4 mm; wavelength range 190–600 nm; 1 nm step and scan speed 50 nm/min. Contributions from the solvent and the quartz cells were subtracted from all the spectra.

■ THEORETICAL METHODS

Structures of all isomers were optimized at the Becke's three parameter exchange Lee, Yang, and Parr correlation (B3LYP)^{36–38} level of theory using the 6-31G*³⁹ basis set under a C_1 geometry. Excited-state energies, oscillator strengths, and velocity rotatory strengths for AXF-155 were calculated using time-dependent density functional theory (TD-DFT),^{40,41} specifically DFT/B3LYP and 6-31G* basis

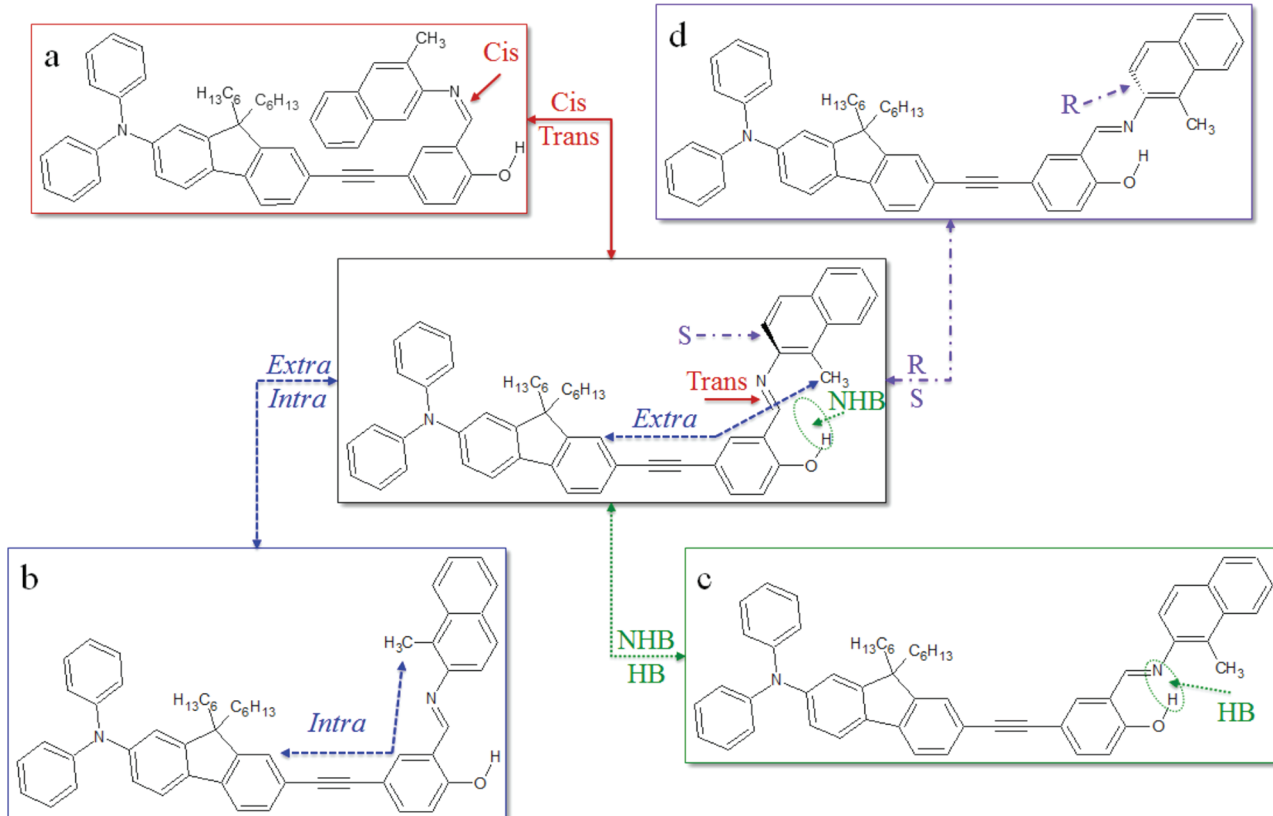


Figure 1. (no hydrogen bonding (NHB)) *trans-S*-extra conformer of AXF-169' (center). (a) (NHB) *cis-M*-extra conformer of AXF-169', (b) (NHB) *trans-R*-intra conformers of AXF-169', (c) (hydrogen bonding (HB)) *trans-S*-extra conformer of AXF-169', and (d) (HB) *trans-R*-extra conformers of AXF-169'.

set, over the first 100 electronic excited states. Calculation on AXF-169' was performed over the first 60 electronic excited states. The polarizable continuum model (PCM),^{42,43} using universal force field (UFF) radii with a multiplicative factor of 1.1, was employed to include solvent effects for both the geometry optimizations and the TD-DFT calculations. We used the nonequilibrium regime for THF with a static dielectric constant of 7.4257 and an optical dielectric constant of 1.9740.

All the calculated electronic transitions were broadened using Gaussian shaped functions with 3500 cm^{-1} (HW(1/e)M) for the absorption spectra and 0.35 eV (HW(1/e)M) for the ECD spectra. The values of $\varepsilon_i(\nu)$ were calculated using the oscillator strength according to⁴¹

$$\begin{aligned}\varepsilon(\nu) &= \sum_{i=1}^n \varepsilon_i(\nu) \\ &= \sum_{i=1}^n \left(\frac{f_i}{7.653619415 \times 10^{-9} \sigma} e^{-\left(\frac{\nu - \nu_i}{\sigma}\right)^2} \right)\end{aligned}\quad (1)$$

The $\Delta\varepsilon_i(\nu)$ (ECD) was obtained from the velocity rotatory strength applying the Harada-Nakanishi equations:⁴⁴

$$\begin{aligned}\Delta\varepsilon(\nu) &= \sum_{i=1}^n \Delta\varepsilon_i(\nu) \\ &= \sum_{i=1}^n \left(\frac{R_i}{2.296 \times 10^{-39} \sqrt{\pi}} \frac{\nu_i}{\sigma} e^{-\left(\frac{\nu - \nu_i}{\sigma}\right)^2} \right)\end{aligned}\quad (2)$$

Here, the i subscript refers to the particular excited state; ν_i is the transition frequency (cm^{-1}) of the excited state of interest, ν is the incident radiation frequency (in cm^{-1}), σ is the standard deviation of the simulated band in wavenumber (HW1/eM) (cm^{-1}), f_i is the oscillator strength (dimensionless), and R_i is the velocity rotatory strength ($\text{erg}\cdot\text{esu}\cdot\text{cm}/\text{Gauss}$) for the corresponding transition. The values of $\varepsilon_i(\nu)$ and $\Delta\varepsilon_i(\nu)$ have units of $\text{l}\cdot\text{mol}^{-1}\cdot\text{cm}^{-1}$.^{45,46}

All the theoretical calculations were performed with Gaussian 09 computational chemistry software.⁴⁷

RESULTS AND DISCUSSION

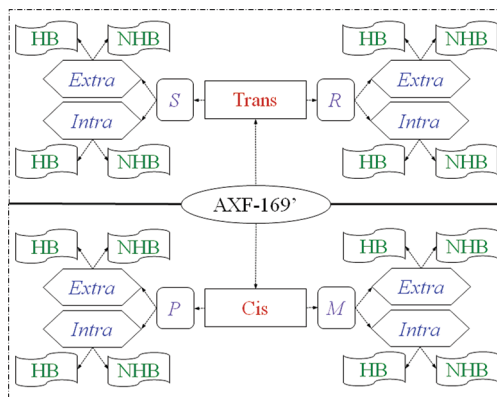
To accurately determine the structure of our novel axially chiral binaphthyl fluorene based salen ligand in THF solution, we performed a systematic comparison of the theoretical ECD spectra of all the potential conformers with the experimental spectrum. For that purpose, we optimized first the molecular structures of half-AXF-155 (AXF-169') in THF according to the procedure explained previously in the theoretical methods. In AXF-169', we replaced one-half of the molecule by a methyl group with the purpose of recognizing the relative orientation of the remaining fluorene moiety with respect to the detached half (see Figure 1).

From these preliminary calculations, we identified the following four significant features on AFX-169': (a) The existence of geometric isomers around the $\text{C}=\text{N}$ bond at the center of the molecule (Figure 1a), (b) the relative orientation of the salicaldehyde moiety with respect to the detached half (pseudo-endo and pseudo-exo isomerism, hereafter, intra and extra, respectively) (Figure 1b), (c) the possibility of formation

of intramolecular hydrogen bonding (HB) (Figure 1c), and (d) the presence of an additional axial chirality around the C=N bond at the center of the molecule (Figure 1d). Despite the existence of the cis isomers, we only show the trans in Figure 1 to illustrate clearly these four features. A similar type of variant was found in the cis isomers.

While geometric isomerism was entirely anticipated, the existence of an intra isomer was a little surprising keeping in mind that the potential steric effects between the two halves in the whole AXF-155 would keep the structure open in an extra arrangement. However, upon replacing one of the halves by a methyl group in AXF-169', these effects can be considered substantially reduced thus opening possibilities for the formation of the intra conformers. The formation of intramolecular HB was also expected because of the close distance between the nitrogen attached to the naphthalene and the hydroxyl group. However, the presence of the additional axial chirality was totally unexpected considering the typical rigidity that the strong π -conjugation conferred to the whole molecular system. This effect, in principle, should maintain the structure planar. Nevertheless, a dihedral angle of $\approx 32^\circ$ for the *trans_R-intra* and $\approx 53^\circ$ for the *trans_R-extra* isomer, for example, showed the contrary. Similar results were also obtained for the cis isomer but with M and P chirality. As a result, there were 16 different distinguishable conformers of AXF-169' to study (Scheme 2). To simplify the classification of such a big number

Scheme 2. Descriptive diagram for the determination of the 16 conformers of AXF-169'. The diagram includes two geometric isomers (trans and cis), four axial chiralities [two for trans (R and S) and two for cis (M and P)], two relative orientations (intra and extra isomerism), and the formation or not of intramolecular hydrogen bonding, HB and NHB, respectively



of molecules, we utilized the following systematic rule: first, we identify the geometric isomer; second, we classify the conformers by optical isomers; and third, we differentiate the relative orientation of the fluorene moiety. For instance, the molecule at the center of Figure 1 would be thus called *trans_S-extra*. The classification with HB or without hydrogen bonding (NHB) is done separately from this methodical assignation of names to the conformers.

To corroborate our theoretical predictions, we synthesized AXF-169 (see Materials and Synthetic Procedures). According to the ^1H NMR characterization of this molecule, the single signal with a chemical shift of 13.64 ppm for the hydroxyl hydrogen is definitely an indication of the absence of intramolecular HB in AXF-169.⁴⁸ This piece of information

reveals the impact of solvent effects in solution and serves to reduce the number of possible conformers of AXF-169 from 16 to only 8. Nevertheless, the theoretical analysis was still performed on all 16 conformers.

Since the absorption spectra of two optical isomers are identical,⁴⁹ in Figure 2a, we show the theoretical absorption spectra of only one enantiomer (R and M for the trans and cis isomers, respectively) of AXF-169, that is, (i) *trans_R-extra*, (ii) *trans_R-intra*, (iii) *cis_M-extra*, and (iv) *cis_M-intra*, with and without HB. The first observation is that the theoretical spectra for all the conformers match well with the experimental within the uncertainty. The observed similarity indicates that the electronic transitions are primarily determined by the conjugated fluorene-alkyne_bond-phenyl_ring branch. The second observation is that the theoretical molar extinction coefficient is slightly larger than the experimental. This small difference is justified considering the size of the molecule under study.

In Figure 2b, we present the theoretical ECD spectra of the same conformers. Because the ECD spectra of optical isomers are mirror images, only the spectrum of one enantiomer is shown. The spectra of equal geometric isomers look alike independently of their relative orientation intra or extra. This indicates that the substitution of half of AXF-155 in AXF-169', by a small methyl group, does not distort substantially the 3D configuration of the latter by changing its relative orientation. Another aspect to be noticed in Figure 2b is the remarkable differences between the ECD spectra of similar structures with and without HB. The clear difference between both reveals the potential of using ECD for the accurate determination of the existence (partial or total) or not of HB in the final 3D molecular structure of AXF-169' and, therefore, of AXF-155. With the intention of corroborating these theoretical results, we attempted to make a comparison between them and the experimental. However, the experimental ECD spectrum was not measurable because of the formation of a racemic mixture of AXF-169 through its synthesis, which was impossible to separate. Nevertheless, the optimization of all conformers revealed strong steric hindrances in the cis isomers. Therefore, one should expect the trans isomer to define the final 3D structural configuration of AXF-155 in solution.

With this information in hand, we proceeded to construct all the possible conformers of AXF-155 combining the different configurations obtained for AXF-169'. Then, we completed the structural optimization of all its conformers and calculated their excited states. Not surprisingly, we found in AXF-155 the same different features already discussed for AXF-169' but in either a symmetric or a dissymmetric fashion with respect to the (R)-(+)-1,1'-binaphthalene moiety at the center of the molecule (Figure 3). Following this approach, we were able to recognize 40 different possible conformers of AXF-155 (see Table 1), 20 with HB and 20 NHB. According to the spectroscopic characterization of AXF-155 using ^1H NMR, the presence of intramolecular HB at the center of the molecule is now an open possibility since a signal with a chemical shift of 12.37 ppm,⁴⁸ for the hydroxyl hydrogen, is too low to completely discard this possibility.

To have a better initial idea of the most probable 3D conformation of AXF-155, we first ran in collaboration with professor Prasad Polavarapu (Professor of Chemistry, Department of Chemistry, Vanderbilt University) molecular dynamic calculations using CONFLEX in gas phase.^{49–51} This first attempt revealed that out of the 90 conformers generated by

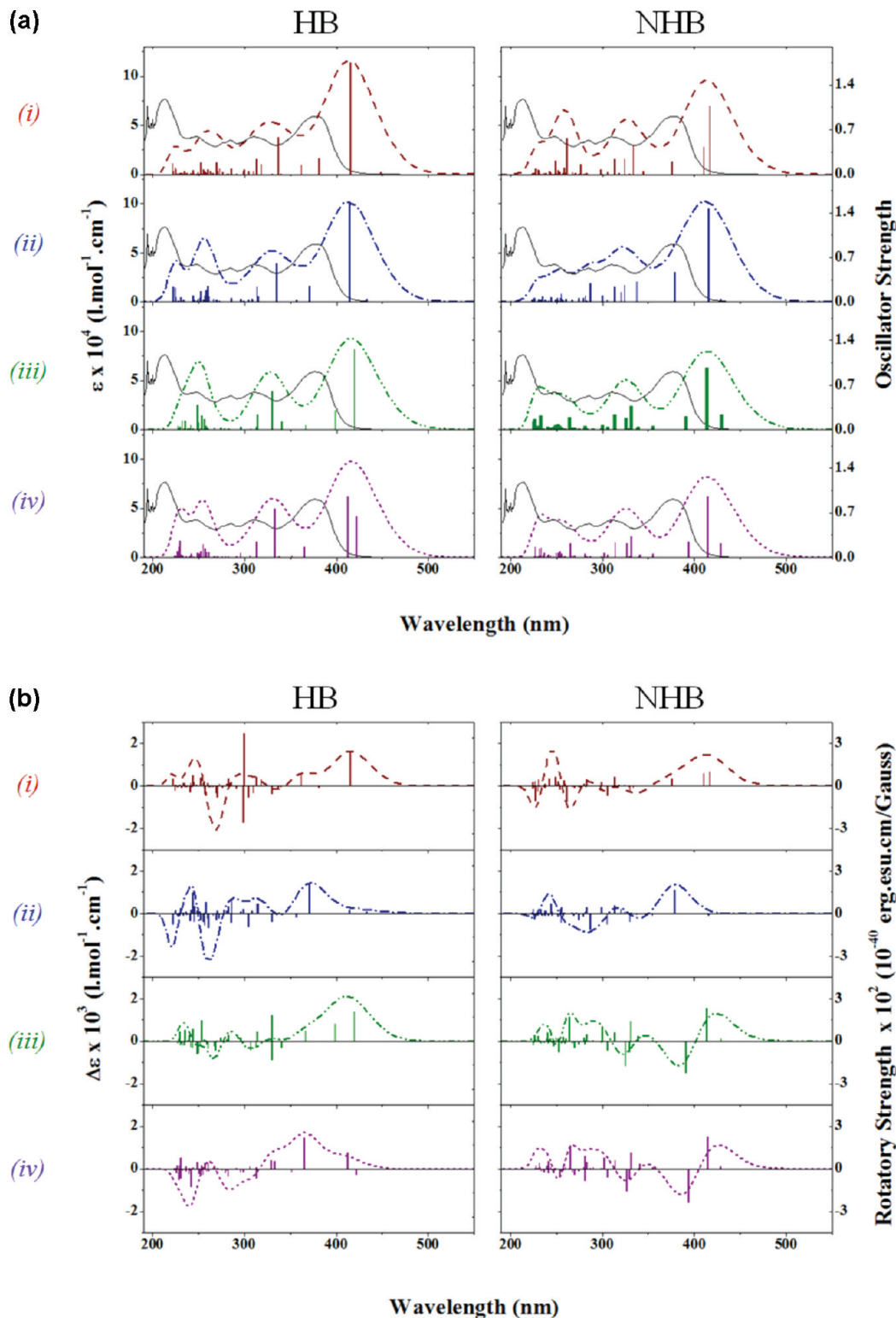


Figure 2. (a) Theoretical (broken lines) and experimental (solid line) UV-vis spectra of AXF-169' conformers. (i) *trans*-R-extra, (ii) *trans*-R-intra, (iii) *cis*-M-extra, and (iv) *cis*-M-intra with (HB) and without hydrogen bonding (NHB). Solid vertical bars represent the different electronic transitions with their corresponding oscillator strengths (scale on the right). (b) Theoretical ECD spectra of AXF-169' conformers. (i) *trans*-R-extra, (ii) *trans*-R-intra, (iii) *cis*-M-extra, and (iv) *cis*-M-intra with (HB) and without hydrogen bonding (NHB). Solid vertical bars represent the different transitions with their corresponding rotatory strengths (scale on the right).

this program for AXF-155, with fixed (R)-axial chirality at the center, the *trans*-R-extra//*trans*-R-extra (90.2749%) should be the predominant conformer of AXF-155 followed by the *trans*-R-intra//*trans*-R-extra (3.9273%) and the *trans*-R-

intra//*trans*-R-intra (0.0566%) in that order (Figure 4a) (the double bar, //, at the center of the name represents the (R)-(+) -1,1'-binaphthalene moiety). However, our spectroscopic theoretical and experimental results, shown later in this article,

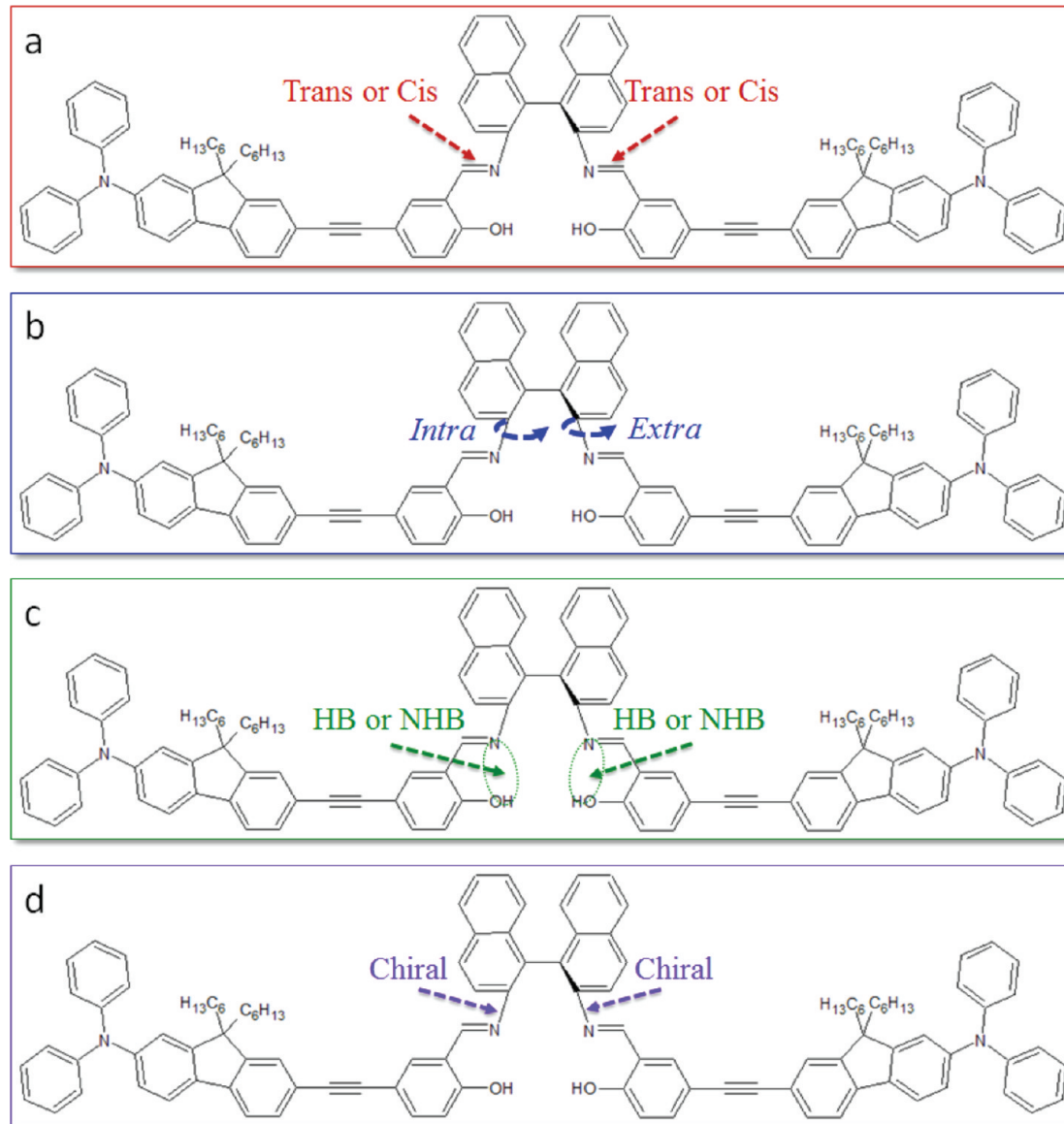


Figure 3. Molecular diagram used for the determination of the 40 conformers of AXF-155, including geometric isomers (trans and cis), relative orientation (intra and extra isomerism), axial chirality, and the formation or not of intramolecular hydrogen bonding (HB and NHB).

Table 1. Symmetric Trans and Cis Conformers of AXF-155

trans-trans conformers	cis-cis conformers
<i>trans_R-intra//trans_R-extra</i>	<i>cis_M-intra//cis_M-extra</i>
<i>trans_S-intra//trans_S-extra</i>	<i>cis_P-intra//cis_P-extra</i>
<i>trans_R-intra//trans_S-extra</i>	<i>cis_M-intra//cis_P-extra</i>
<i>trans_S-intra//trans_R-extra</i>	<i>cis_P-intra//cis_M-extra</i>
<i>trans_R-intra//trans_R-intra</i>	<i>cis_M-intra//cis_M-intra</i>
<i>trans_S-intra//trans_S-intra</i>	<i>cis_P-intra//cis_P-intra</i>
<i>trans_S-intra//trans_R-intra</i>	<i>cis_P-intra//cis_M-intra</i>
<i>trans_R-extra//trans_R-extra</i>	<i>cis_M-extra//cis_M-extra</i>
<i>trans_S-extra//trans_S-extra</i>	<i>cis_P-extra//cis_P-extra</i>
<i>trans_S-extra//trans_R-extra</i>	<i>cis_P-extra//cis_M-extra</i>

clearly demonstrate that the only species present in the THF solution is the *trans_R-intra//trans_R-extra*.

To explain this discrepancy is good to remember that calculations of steric energies using molecular dynamics only consider intramolecular interactions (bond stretching, bond bending and bond torsional forces, van der Waals and

electrostatic interactions).⁵² Therefore, the geometry optimization essentially depends on the input structure (in this particular case AXF-155) and not on how other effects such as intermolecular steric hindrances between the interacting parts (AFX-147 and (*R*)-(+)2,2'-diamino-1,1'-binaphthalene) can favor the formation of a particular conformer throughout the chemical reaction. Hence, the synthesis of a conformer such as the *trans_R-extra//trans_R-extra* with a relative lower energy in the potential energy surface (PES) is impeded by the mentioned effect thus favoring the formation of another conformer with a relative higher energy in PES, that is, the *trans_R-intra//trans_R-extra*. This is consistent with our empirical examination of the different possibilities for the nucleophilic addition of (*R*)-(+)2,2'-diamino-1,1'-binaphthalene to the carbonyl carbon of salicaldehyde AXF-147 shown at the end of this article.

An additional interesting outcome from the molecular dynamic calculations is the presence of intramolecular HB between the hydroxyl group and the adjacent nitrogen of the

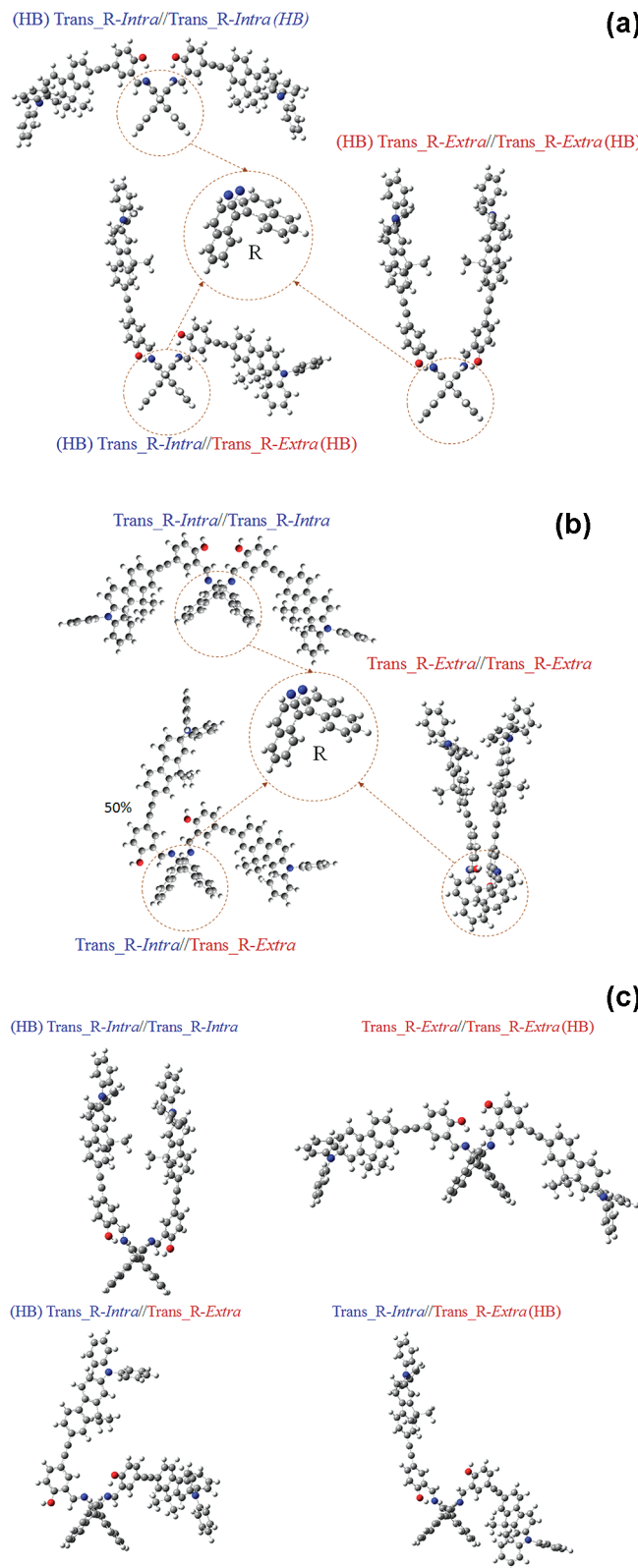


Figure 4. (a) Optimized 3D molecular structure of AXF-155 with HB at both sides, *trans*-R-intra//*trans*-R-intra, *trans*-R-extra//*trans*-R-extra, and *trans*-R-intra//*trans*-R-extra. (b) Optimized 3D molecular structure of AXF-155 in *trans*-R-intra//*trans*-R-intra, *trans*-R-extra//*trans*-R-extra, and *trans*-R-intra//*trans*-R-extra conformation with NHB at both sides of the molecule. (c) Optimized 3D molecular structure of AXF-155 in *trans*-R-intra//*trans*-R-intra and *trans*-R-

Figure 4. continued

extra//trans-R-extra with HB in only one side of the molecule and in *trans*-R-intra//*trans*-R-extra with HB in only one side of the molecule.

diphenylamino on each half of AXF-155 in the gas phase. This result was not unexpected since the proximity between both groups allows for such an interaction. However, in solution, this type of interaction can become weaker by solvent effects, for example, solvation of AXF-155. The discussion about the characterization of AXF-169 supports this statement. Nonetheless, we still considered the three conformers with HB at both sides (Figure 4a), the three with NHB (Figure 4b), and the four asymmetric HB species, that is, with HB in only one side of AXF-155 (Figure 4c). An additional structure not included in the discussion but with 5.6733% probability, according to CONFLEX calculations, is the *trans*-S-intra//*trans*-S-extra. This specific and unexpected conformer was totally discarded because its theoretical ECD spectrum was totally inverted with respect to the experimental (see Supporting Information).

In Figure 5a, we show the experimental absorption spectrum of AXF-155 and the theoretical absorption spectra of the *trans*-R-intra//*trans*-R-intra and the *trans*-R-extra//*trans*-R-extra 3D structures in THF solution. It can be noticed that the spectral shapes and the molar extinction coefficients of all of them are very similar for the same reasons explained before in the discussion of Figure 2a. Therefore, one cannot rely on this data to identify the actual configuration of AXF-155. Nevertheless, the shape and the differences in amplitude observed between the experimental absorption spectra of AXF-169 and that of AXF-155 (approximately 2 folds greater for AXF-155) lead us to think that because the π -electron conjugation is broken at the center of AXF-155, the electronic transitions of this molecule are mostly determined by the electronic transitions of AXF-169. In an effort to establish the 3D structural configuration of AXF-155 in solution, we collected more theoretical–experimental spectroscopic data. In Figure 5b, we present the experimental ECD spectrum of AXF-155 in THF solution and the theoretical spectra of the same six conformers.

Because of the less steric hindrances found in AXF-169, the open configuration with NHB in that molecule was favored. However, in AXF-155, the constraints imposed by the presence of two bulky AXF-169, attached together by the naphthalene moieties to form AXF-155, impose more restrictions to the molecule's degree of freedom thus favoring the formation of intramolecular HB in the gas phase. However, in THF, this interaction seems to become weaker thus permitting the formation of species with NHB.

Using ECD, a technique that has been proven to be very sensitive to 3D molecular structural conformations,⁴⁴ we were able to discard the *trans*-R-extra//*trans*-R-extra and the *trans*-R-intra//*trans*-R-intra. This was done through the cautious comparison of the theoretical and experimental ECD spectra of the AXF-155 shown in Figure 5b. As it can be seen, while in all the *trans*-R-extra//*trans*-R-extra the principal theoretical peak–valley feature between 350 and 450 nm is inverted, in the *trans*-R-intra//*trans*-R-intra there is (a) no valley between 400 and 450 nm for the conformer with HB at both sides of the molecule (Figure 5b, i); (b) a strong spectral

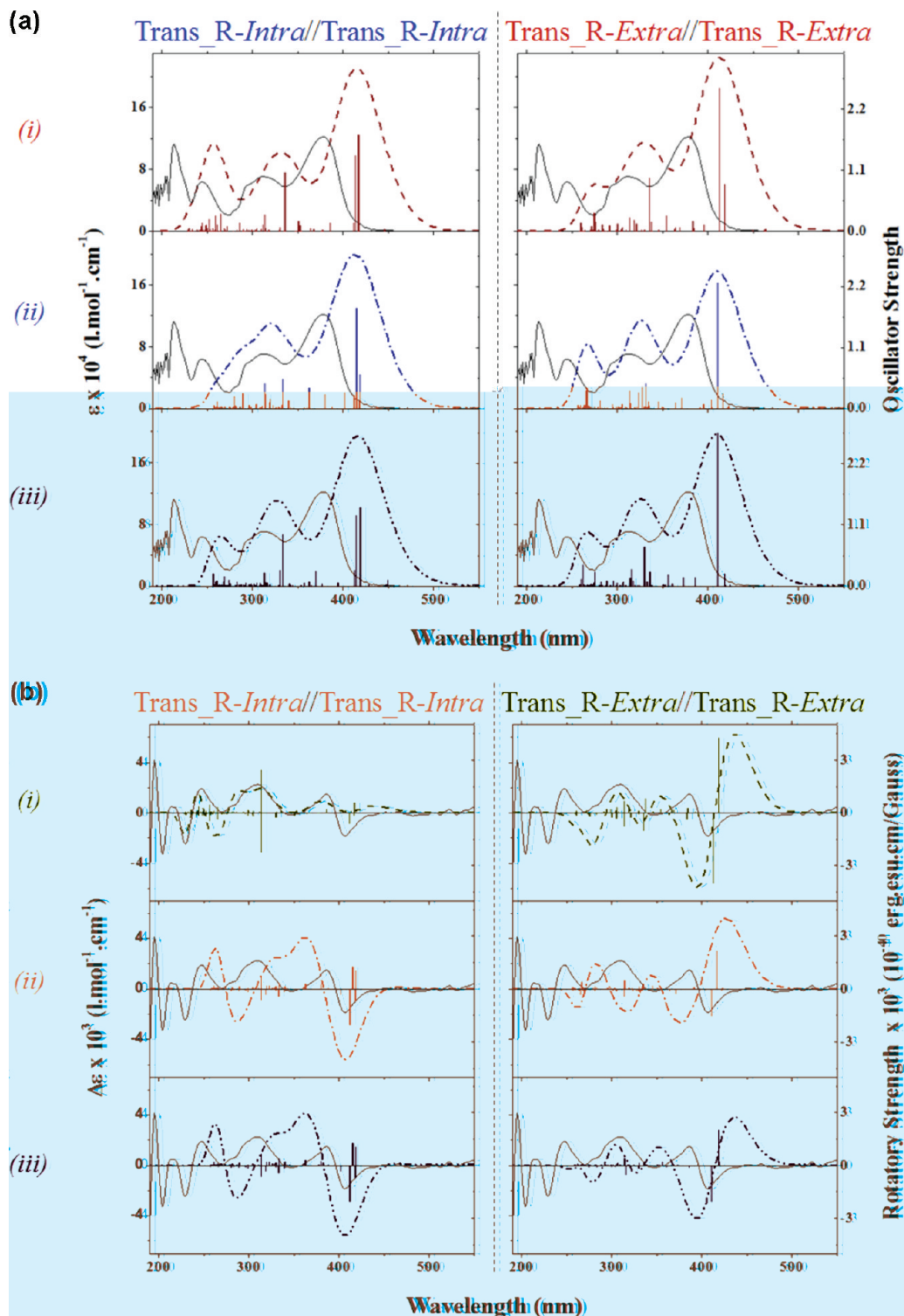


Figure 5. (a) Theoretical (broken lines) and experimental (solid line) UV-vis spectra of the two symmetric AXF-155 conformers, *trans-R-intra//trans-R-intra* and *trans-R-extra//trans-R-extra*, with (i) HB at both sides, (ii) NHB, and (iii) HB in only one side of the molecule. Solid vertical bars represent the different transitions with their corresponding oscillator strength (scale on the right). (b) Theoretical (broken lines) and experimental (solid line) ECD spectra of the two symmetric AXF-155 conformers, *trans-R-intra//trans-R-intra* and the *trans-R-extra//trans-R-extra*, with (i) HB at both sides, (ii) NHB, and (iii) HB in only one side of the molecule. Solid vertical bars represent the different transitions with their corresponding rotatory strength (scale on the right).

blue-shift of the longer wavelength positive band accompanied by the appearance of a negative band at ca. 290 nm for conformer with NHB (Figure 5b, ii); and (c) no strong features between 250 and 450 nm and a significant peak/valley

amplitude disproportion in the red region of the spectral range for the dissymmetric conformer with HB in only one-half of the molecule (Figure 5b, iii). (In the Supporting Information, we show the oscillator and rotatory strength for

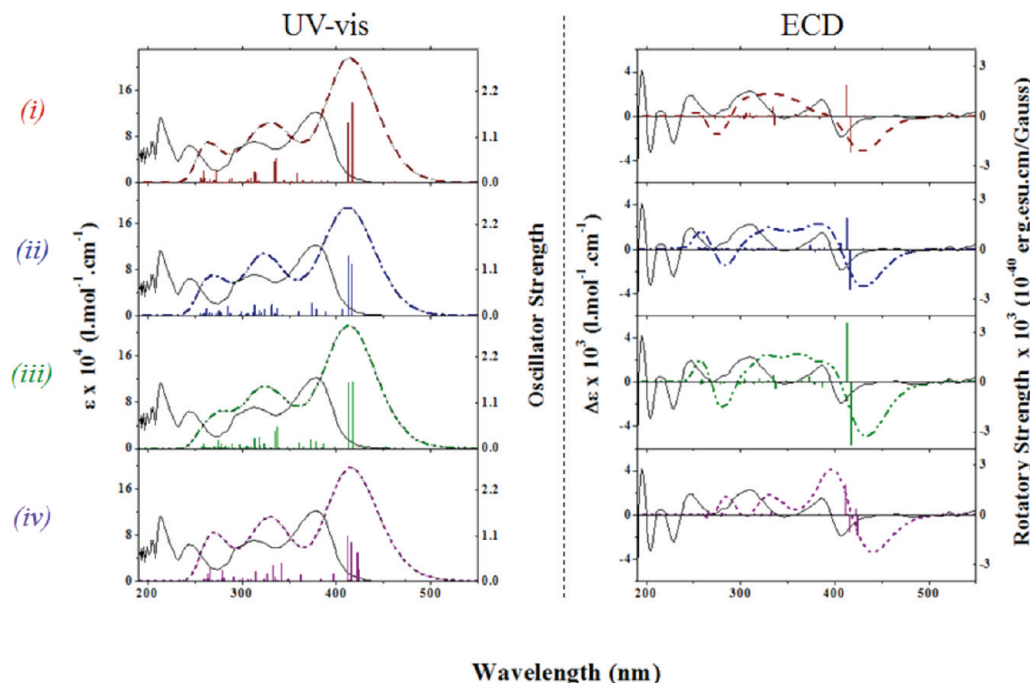


Figure 6. Theoretical (broken lines) and experimental (solid line) UV-vis and ECD spectra of the asymmetric AXF-155 conformer, *trans-R-intra//trans-R-extra*, with (i) HB at both sides, (ii) NHB, (iii) HB only in the *trans-R-extra* side, and (iv) HB only in *trans-R-intra* side. The oscillator strength and the rotatory strength scales are on the right of the graphs.

the first 20 transitions of these six conformations.) These clear theoretical–experimental differences are evidence to discard the 6 symmetric conformers from the list of 10 possible 3D structural conformations of AXF-155 in THF solution. It also suggests that the ultimate structure should be a combination of *trans-R-intra* and *trans-R-extra*. In fact, there is only one remaining candidate, the *trans-R-intra//trans-R-extra* conformer.

In Figure 6, we show the experimental and theoretical absorption and ECD spectra of the four asymmetric *trans-R-intra//trans-R-extra* configurations in THF solution with and without HB. First, one can notice that the theoretical absorption spectra of all four arrangements are very similar among them and are similar to the experimental as discussed above. However, discerning between the four different configurations of this conformer, with and without HB, using ECD is a difficult task because the theoretical and experimental spectra match satisfactorily for all of them. Noticeably, the best theoretical–experimental pairing is observed for the configuration with NHB (Figure 6ii) and that with HB on *trans-R-intra* (Figure 6iv). The strong spectral resemblance leads us to think that these should be the preferred 3D structural conformation of AXF-155 in THF solution. However, the other two configurations of the same *trans-R-intra//trans-R-extra* conformer might be present in this solution. Consequently, one cannot reject the presence of any of the other two in THF and at room temperature. In an effort to discern between all four possibilities, we calculated the energies and entropies of these four structures (see Table 2). As one can see in Table 2, the energies are virtually identical for all four possibilities and are only slightly lower for that with HB at both sides (Figure 6i).

To obtain a better grasp of the actual fractions of all probable species in THF solution, we calculated the Boltzmann weighted average for all of them using the energies in Table 2. The

Table 2. Calculated Energies and Entropies and Boltzmann Weighted Average^a of the Four Asymmetric Conformers of AXF-155 (*trans-R-intra//trans-R-extra*) with HB at Both Sides, NHB, HB Only in the *trans-R-extra* Side, and HB Only in *trans-R-intra* Side

	conformer	energy (Ha)	entropy (J/mol.K)	Boltzmann weighted average ^a
i	(HB) <i>trans-R-intra//trans-R-extra</i> (HB)	-3915.004	1900.477	0.999991
ii	<i>trans-R-intra//trans-R-extra</i>	-3,914.977	1910.117	3.74908×10^{-13}
iii	<i>trans-R-intra//trans-R-extra</i> (HB)	-3914.985	1899.331	1.80187×10^{-9}
iv	(HB) <i>trans-R-intra//trans-R-extra</i>	-3914.993	1791.731	8.66010×10^{-6}

$$^a n_i/N = e^{-E_i/kT} / \sum_i e^{-E_i/kT}$$

Boltzmann probability of occurrence suggests that the conformer with HB at both sides (Figure 6i) should have an overwhelming contribution of 99.9991%. However, this result is not conclusive since the ECD spectra of the other three conformers resemble much better the experimental ECD spectrum of AXF-155. In addition, other effects such as the important steric hindrance between the interacting parts and solvation effects could favor the formation of configurations ii and iv of the *trans-R-intra//trans-R-extra* conformer through the condensation phase of the reaction.

Having determined the structural configuration of AXF-155, we inspected the different possibilities for the nucleophilic addition of (*R*)-(+)-2,2'-diamino-1,1'-binaphthalene to the carbonyl carbon of salicaldehyde AXF-147 following the well-known Burgi:Dunitz trajectory.¹⁹ This empirical examination, supported by our theoretical–experimental results, confirms the formation of the sole *trans-R-intra//trans-R-extra* conformer.

In a first stage, the steric impediment coming from one of the naphthalene amino moieties in the nucleophile forces the attack to take place at approximately $105^\circ \pm 5^\circ$ with respect to the C=O through the electron pair of the most accessible nitrogen, that is, from below (Figure 7a, left side). Although this attack can take place through either side of the molecule, it always ends forming the *trans_R-intra* conformer. The alternative possibilities of attack from above were found to be not viable because of the strong steric hindrances imposed by the nucleophile or AXF-147, which restricts the interaction between the two molecules (Figure 7b, right side).

In a second stage, the consecutive attack of the generated species in stage 1 to another AXF-147 materializes following the same type of trajectory.¹⁹ Since the steric effects are now more obstructive than in the first stage, the attack is more likely to happen from below through the left side of the molecule and from the above through the right (Figure 7b). This molecular positioning only generates the *trans_R-extra* on that side (Figure 7b). As a result, the unequivocal generated conformer is indeed the *trans_R-intra*//*trans_R-extra*. Remarkably, these two steps result in the same conformer independently of the chances of starting with an AXF-147 with or without HB. Therefore, there is an apparent possibility of finding all four different configurations (with and without HB) of this conformer in solution.

In an attempt to explain the discrepancy between the preferential configuration of the *trans_R-intra*//*trans_R-extra* conformer, yielded by the Boltzmann weighted average (Figure 6i) and that obtained by comparing the overlapping between the theoretical and experimental ECD spectra (Figure 6iv), we examined the influence of solvent effects throughout the reaction. It is known that intramolecular hydrogen bonding on the carbonyl oxygen can increase the electrophilicity of the carbonyl group thus making it more reactive.⁵³ On the basis of this statement, the presence of this type of interaction in AXF-147 should favor the formation of the *trans_R-intra*//*trans_R-extra* conformer with HB at both sides. However, in protic solvents, this interaction can be counteracted by the solvation of the hydroxyl proton on the electrophile.⁵⁴ Consequently, having used ethanol as a solvent in the last step of the synthesis of AXF-155 and considering the solvation of the hydroxyl proton on AXF-147, one should attain a preferential formation of the *trans_R-intra*//*trans_R-extra* conformer of AXF-155 with NHB. Therefore, the conformer with NHB at both sides should be the dominant configuration in solution. However, the spectral resemblance between the theoretical and the experimental ECD spectra of all four configurations indicates the presence of a mixture of all of them in solution.

Although discerning between the four different configurations of this conformer in solution is very challenging, we can be certain of two things: (a) the only conformer of AXF-155, present in THF solution, is the *trans_R-intra*//*trans_R-extra* and (b) the most favored configuration in THF solution should be the *trans_R-intra*//*trans_R-extra* conformer with NHB (Figure 6ii).

CONCLUSIONS

Throughout the theoretical–experimental analysis of the ECD spectrum of this novel axially chiral binaphthyl fluorene based salen ligand and by inspecting the different possibilities for the nucleophilic addition of (*R*)-(+)2,2'-diamino-1,1'-binaphthalene to the carbonyl carbon of salicaldehyde AXF-147 following the well-known Burgi:Dunitz trajectory, we were able to determine

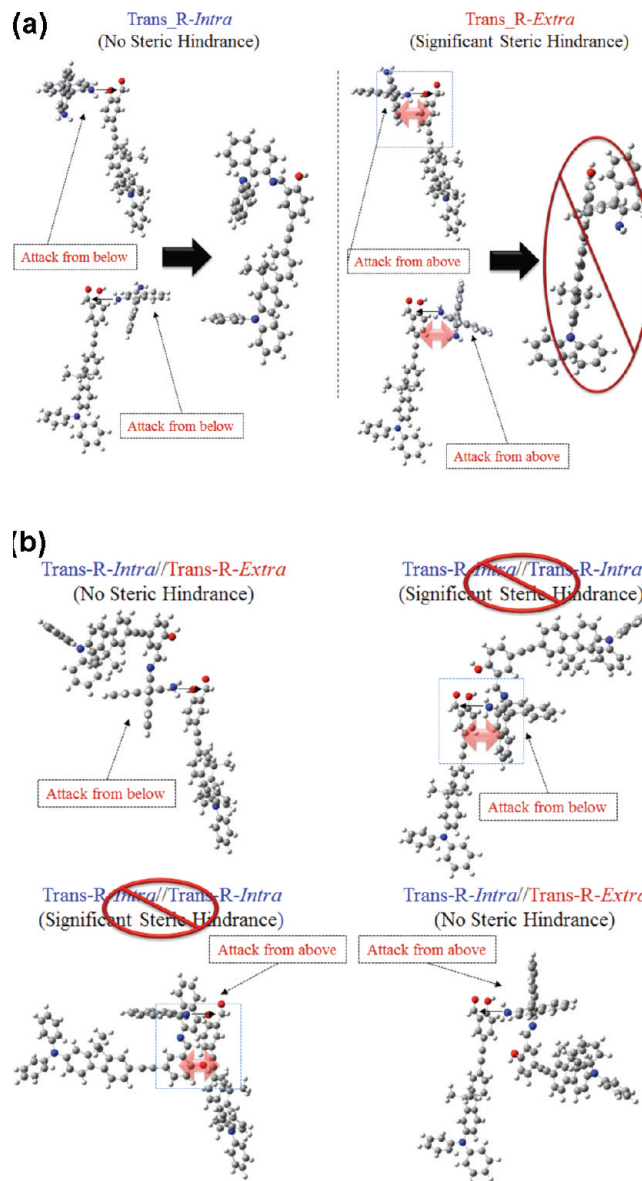


Figure 7. (a) Representation of the naphthalene amino moiety (nucleophile) attack to AXF-147 from different flanks of the salicaldehyde derivative following a Burgi:Dunitz trajectory. Top-left: attack through the left side of AXF-147 with the nitrogen that is attached to the naphthalene placed underneath; bottom-left: attack through the right side of AXF-147 with the nitrogen that is attached to the naphthalene placed underneath; top-right: attack through the left side of AXF-147 with the nitrogen that is attached to the naphthalene placed above; bottom-right: attack through the right side of AXF-147 with the nitrogen that is attached to the naphthalene placed above. Thin arrows show the attack site. Thick semitransparent double arrows indicate steric hindrance. (b) 3D description of the attack of the naphthalene amino-AXF-147 fragment to another AXF-147 from different flanks and following a Burgi:Dunitz trajectory. Top-left: attack through the left side of AXF-147 with the available nitrogen attached to the naphthalene placed underneath; bottom-left: attack through the left side of AXF-147 with the available nitrogen that is attached to the naphthalene placed above; top-right: attack through the right side of AXF-147 with the available nitrogen that is attached to the naphthalene placed underneath; bottom-right: attack through the right side of AXF-147 with the available nitrogen that is attached to the naphthalene placed above. Thin arrows show the attack site. Thick semitransparent double arrows indicate steric hindrance.

the 3D structural conformation of AXF-155 in a THF solution. ECD has been proven to be a powerful tool to provide accurate information not only about the structure of organic molecules with extended π -electron conjugation but also of molecules with multiple axial chiralities in solution. AXF-155 is expected to find potential applications in homogeneous catalysis, biophotonics, and sensing. Work in the sensing applications is in progress.

■ ASSOCIATED CONTENT

S Supporting Information

3D molecular structure, UV-vis, and ECD spectra of the *trans-S-intra//trans-S-extra* conformer. Tables with the oscillator and rotatory strengths of the first 20 excited states of the 10 main conformers of AXF-155, i.e., *trans-R-extra//trans-R-extra*, *trans-R-intra//trans-R-intra*, and *trans-R-intra//trans-R-extra*. This material is available free of charge via the Internet at <http://pubs.acs.org>.

■ AUTHOR INFORMATION

Notes

The authors declare no competing financial interest.

■ ACKNOWLEDGMENTS

This work was partially supported by the National Science Foundation through grant no. CHE-0832622. The authors would like to acknowledge Dr. Suren Tatulian, Assistant Professor, Physics Department at UCF, for kindly allowing them to measure the experimental ECD spectrum of AXF-155 in his J-810 CD spectropolarimeter. F.E. Hernandez would like to thank Professor Prasad Polavarapu, Professor of Chemistry, Department of Chemistry, Vanderbilt University, for his valuable support performing the molecular dynamic calculations of AXF-155 in gas phase using CONFLEX.

■ REFERENCES

- (1) *Comprehensive Asymmetric Catalysis*; Pfaltz, A.; Jacobsen, E. N., Yamamoto, H., Eds.; Springer: New York, 1999; Vols. 1–3.
- (2) Kitamura, M.; Tokunaga, M.; Ohkuma, T.; Noyori, R. *Org. Synth.* **1993**, *71*, 1–9.
- (3) *Chirality in Industry*; Akutagawa, S., Ed.; Wiley: London, 1992.
- (4) Kumabayashi, H.; Sayo, N.; Akutagawa, S.; Sakaguchi, T.; Tsuruta, H. *Nippon Kagaku Kaishi* **1997**, *12*, 835–846.
- (5) Cozzi, P. G. *Chem. Soc. Rev.* **2004**, *33*, 410–421.
- (6) Baileza, C.; Garcia, H. *Chem. Rev.* **2006**, *106*, 3987–4043.
- (7) Katsuki, T. *Adv. Synth. Catal.* **2002**, *344*, 131–147.
- (8) Cozzi, P. G. *Angew. Chem., Int. Ed.* **2003**, *42*, 2895–2898.
- (9) Pathak, K.; Bhatt, A. P.; Abdi, S. H. R.; Kureshy, R. I.; Khan, N. H.; Ahmad, I.; Jasra, R. *Chirality* **2007**, *19*, 82–88.
- (10) Wezemberg, S. J.; Kleij, A. W. *Angew. Chem., Int. Ed.* **2008**, *47*, 2354–2364.
- (11) Kleij, A. W. *Chem.—Eur. J.* **2008**, *14*, 10520–10529.
- (12) Di Mauro, E. F.; Kozlowski, M. C. *Org. Lett.* **2001**, *3*, 3053–3056.
- (13) Jiang, C. J.; Chen, Z. R. *Kinet. Catal.* **2008**, *49*, 474–478.
- (14) Rozenberg, V.; Kharitonov, V.; Antonov, D.; Sergeeva, E.; Aleshkin, A.; Ikonnikov, N.; Orlova, S.; Belokon, Y. *Angew. Chem.* **1994**, *106*, 106–108.
- (15) Danilova, T. I.; Rozenberg, V. I.; Starikova, Z. A.; Bräse, S. *Tetrahedron: Asymmetry* **2004**, *15*, 223–229.
- (16) Wiznycia, A. V.; Desper, J.; Levy, C. J. *Chem. Commun.* **2005**, 4693–4695.
- (17) Mukherjee, C.; Stammmer, A.; Bögge, H.; Glaser, T. *Chem.—Eur. J.* **2010**, *16*, 10137–10149.
- (18) MacMillan, S. N.; Jung, C. F.; Shalumova, T.; Tanski, J. M. *Inorg. Chim. Acta* **2009**, *362*, 3134–3146.
- (19) Bürgi, H. B.; Dunitz, J. D.; Lehn, J. M.; Wipff, G. *Tetrahedron* **1974**, *30*, 1563–1572.
- (20) Hernández, F. E.; Belfield, K. D.; Cohanoschi, I. *Chem. Phys. Lett.* **2004**, *391*, 22–26.
- (21) Cohanoschi, I.; Belfield, K. D.; Hernández, F. E. *Chem. Phys. Lett.* **2005**, *406*, 462–466.
- (22) Hernández, F. E.; Belfield, K. D.; Cohanoschi, I.; Balu, M.; Schafer, K. J. *J. Appl. Opt.* **2004**, *43*, 5394–5398.
- (23) Belfield, K. D.; Morales, A. R.; Kang, B. S.; Hales, J. M.; Hagan, D. J.; Van Stryland, E. W.; Chapela, V. M.; Percino, J. *Chem. Mater.* **2004**, *16*, 4634–4641.
- (24) Belfield, K. D.; Schafer, K. J.; Mourad, W.; Reinhardt, B. A. *J. Org. Chem.* **2000**, *65*, 4475–4481.
- (25) Hales, J. M.; Hagan, D. J.; Van Stryland, E. W.; Schafer, K. J.; Morales, A. R.; Belfield, K. D.; Pacher, P.; Kwon, O.; Zojer, E.; Bredas, J.-L. *J. Chem. Phys.* **2004**, *21*, 3152–3160.
- (26) Belfield, K. D.; Bondar, M. V.; Przhonska, O. V.; Schafer, K. J. *Photochem. Photobiol. A* **2004**, *162*, 489–496.
- (27) Belfield, K. D.; Bondar, M. V.; Przhonska, O. V.; Schafer, K. J. *Photochem. Photobiol. A* **2004**, *162*, 569–574.
- (28) Belfield, K. D.; Bondar, M. V.; Przhonska, O. V.; Schafer, K. J. *Photochem. Photobiol. Sci.* **2004**, *3*, 138–141.
- (29) Schafer, K. J.; Belfield, K. D.; Yao, S.; Frederiksen, P. K.; Hales, J. M.; Kolattukudy, P. E. *J. Biomed. Opt.* **2005**, *10*, 051402-1–051402-8.
- (30) Cohanoschi, I.; Toro, C.; Hernandez, F. E. *J. Chem. Phys.* **2006**, *124*, 194707-1–194707-5.
- (31) Andrasik, S. J.; Belfield, K. D.; Bondar, M. V.; Hernández, F. E.; Morales, A. R.; Przhonska, O. V.; Yao, S. *ChemPhysChem* **2007**, *8*, 399–404.
- (32) Belfield, K. D.; Bondar, M. V.; Yanez, C. O.; Hernández, F. E.; Przhonska, O. V. *J. Mater. Chem.* **2009**, *19*, 7498–7502.
- (33) Chang, K. H.; Lin, Y. C.; Huang, C. C.; Liu, Y. H.; Hu, Y. H.; Chou, P. T. *Dalton Trans.* **2004**, 1731–1738.
- (34) Reinhardt, B. A.; Brott, L. L.; Clarson, S. J.; Dillard, A. G.; Bhatt, J. C.; Kannan, R.; Yuan, L.; He, G. S.; Prasad, P. N. *Chem. Mater.* **1998**, *10*, 1863–1874.
- (35) Morales, A. R.; Belfield, K. D.; Hales, J. M.; Van Stryland, E. W.; Hagan, D. J. *Chem. Mater.* **2006**, *18*, 4972–4980.
- (36) Becke, A. D. *J. Chem. Phys.* **1993**, *98*, 5648–5652.
- (37) Becke, A. D. *Phys. Rev. A* **1988**, *38*, 3098–3100.
- (38) Lee, C.; Yang, W.; Parr, R. G. *Phys. Rev. B* **1988**, *37*, 785–789.
- (39) Hariharan, P. C.; Pople, J. A. *Theor. Chem. Acc.* **1973**, *28*, 213–222.
- (40) Runge, E.; Gross, E. K. U. *Phys. Rev. Lett.* **1984**, *52*, 997–1000.
- (41) Dierksen, M.; Grimme, S. *J. Chem. Phys.* **2006**, *124*, 174301-1–174301-12.
- (42) Tomasi, J.; Mennucci, B.; Cammi, R. *Chem. Rev.* **2005**, *105*, 2999–3093.
- (43) Mennucci, B.; Tomasi, J.; Cammi, R.; Cheeseman, J. R.; Frisch, M. J.; Devlin, F. J.; Gabriel, S.; Stephens, P. J. *J. Phys. Chem. A* **2002**, *106*, 6102–6113.
- (44) *Circular Dichroism: Principles and Applications*; Nakanishi, K.; Berova, N.; Woody, R. W., Eds.; VCH: New York, 1994.
- (45) Chang, K. C.; Su, I. H.; Lee, G. H.; Chung, W. S. *Tetrahedron Lett.* **2007**, *48*, 7274–7278.
- (46) Polavarapu, P. L. *J. Phys. Chem. A* **2005**, *109*, 7013–7023.
- (47) Frisch, M. J.; Trucks, G. W.; Schlegel, H. B.; Scuseria, G. E.; Robb, M. A.; Cheeseman, J. R.; Scalmani, G.; Barone, V.; Mennucci, B.; Petersson, G. A.; et al. *Gaussian 09*, revision A.1; Gaussian, Inc.: Wallingford, CT, 2009.
- (48) Woo, Y.; Koh, D.; Lim, Y. *Magn. Reson. Chem.* **2009**, *47*, 184–189.
- (49) Goto, H.; Osawa, E. *J. Mol. Struct.* **1993**, *285*, 157–168.
- (50) Goto, H.; Osawa, E. *J. Chem. Soc., Perkin Trans. 2* **1993**, 187–198.

- (S1) *Computer Aided Innovation of New Materials*; Doyama, M., Ed.; Elsevier: Amsterdam, 1991.
- (S2) *Computational Chemistry Using the PC*; Rogers, D. W., Editor; Wiley: NJ, 2007.
- (S3) Sadekov, I. D.; Minkin, V. I.; Lutskii, A. E. *Russ. Chem. Rev.* **1970**, *39*, 179–195.
- (S4) Exarchou, V.; Troganis, A.; Gerofhanassis, I. P.; Tsimidou, M.; Boskou, D. *Tetrahedron* **2002**, *58*, 7423–7429.